Molecular evaporation and condensation of liquid *n*-alkane films

Ting Kang Xia and Uzi Landman
School of Physics, Georgia Institute of Technology, Atlanta, Georgia 30332

(Received 25 February 1994; accepted 12 April 1994)

Energetic, structural, and dynamical properties of solid-to-liquid and liquid-to-vapor interfaces and molecular evaporation and condensation processes from high-temperature liquid n-C_6H_{14} and n-$C_{16}H_{34}$ films were investigated with molecular dynamics simulations. For hexadecane all evaporation events occurred via monomers while for hexane, evaporation of monomers as well as dimers were observed. For both alkane liquids the molecular evaporation mechanism is found to be sequential in nature, starting with an end segment of a molecule leaving the surface and subsequently the evaporation of the molecule occurs via sequential "dragging" of the rest of the molecule. The condensation coefficients of vapor molecules onto the liquid surface are estimated as ~0.9 for hexane and ~1 for hexadecane. Evaporation is accompanied by significant molecular conformational changes. In hot liquid n-$C_{16}H_{34}$ the *trans* (t) and *gauch* (g_+ and g_-) dihedral conformations are distributed as $(t,g_+,g_-)=(66,17,17)$ while in the vapor the distribution is almost uniform with a large decrease in the fraction of *trans* conformations, i.e., (33,31,36). On the other hand, for the shorter alkane hot liquid $(t,g_+,g_-)=(72,14,14)$ while in the vapor the fraction of trans conformations is increased, i.e., (83,10,7). These results are discussed in light of theoretical treatments of evaporation processes.

I. INTRODUCTION

Investigations of the thermodynamic, structural, dynamic, rheological, and compositional properties of surfaces and interfaces of complex liquids (e.g., molecular liquids, such as water; paraffins, such as n-alkanes, C_nH_{2n+2}; and polymers) aimed at probing and understanding the molecular mechanisms underlying interfacial phenomena in these systems are an active area of challenging experimental and theoretical research endeavors of fundamental as well as technological significance.[1,2] The structural and dynamical complexities of such liquids are compounded at surfaces and interfaces where the homogeneity of the system is broken. Consequently, it is expected, and indeed found, that the properties of liquids, complex liquids in particular, can be significantly modified at surfaces and interfaces, leading to new behavior such as stratification of the interfacial liquid density ("layering"),[2-6] surface segregation (preferential adsorption) of long-chain molecules from a homogeneous mixture of long- and short-chain molecules,[7,8] the capacity of confined liquids to withstand load,[2,3,6,7(a)] prefreezing phenomena (surface crystallization occurring above the bulk solidification temperature),[9,10] and interfacial interphase transformations during shear,[11] to name a few. Obviously, fundamental understanding of the molecular-level processes of such interfacial phenomena are of importance for a variety of diverse technological applications including formation and properties of adhesive contacts,[6] lubrication,[4,12] coatings, colloidal stability, and flocculation,[13] and biocompatibility of artificial internal organs.

Recent research efforts in the area of interfacial complex liquids focused mainly on interfaces between condensed phases i.e., solid-to-liquid; for recent simulations of liquid-to-vapor interfaces of n-alkanes see Refs. 5, 10, and 14. However, molecular exchange between liquids and the gaseous phase plays an important role in diverse processes; such as drying, steam generation, saline water distillation, sewage concentration, molecular distillation, isotope separation, evaporation of lubricants, cooling by evaporation, hardening of plastics caused by volatilization of softeners, and fuel evaporation.[15]

Liquid evaporation and condensation processes have been observed and studied for a rather long time, with the first systematic investigations on the evaporation process of water dating back to Dalton in 1803,[16] and further studied by Stefan in 1872.[17] Early theories of the exchange rate between a condensed phase (liquid) and its vapor were based on the kinetic theory of gases, starting with Hertz in 1882,[18] leading to a relation between the net evaporation rate (G, expressing the net mass evaporating per unit time and unit area, under isothermal conditions) and the pressures in the liquid (P_l) and vapor (P_v) phases. Assuming equal temperature (T) for the two phases, the Hertz–Knudsen–Langmuir equation (HKL)[19] for G is

$$G=\alpha(P_l-P_v)(M/2\pi RT)^{1/2}, \tag{1}$$

where M is the molar mass, R is the gas constant, and α is the evaporation coefficient, expressing the ratio between the measured and calculated evaporation rates. It should be noted that the above equation was derived only on the basis of the kinetic theory of gases and microscopic reversibility with no consideration of the liquid phase or liquid-to-vapor interface, and it implies several simplifications, including: (i) use of equilibrium molecular distribution functions under nonequilibrium conditions, (ii) no molecular backscattering near the liquid surface, and (iii) application of the ideal gas law to the vapor. Corrections to the above formula, to account for nonequilibrium effects, have also been derived.[20]

Much research in the area of liquid evaporation and condensation kinetics focused on the evaporation coefficient, α defined in Eq. (1), (with a similar definition for the condensation coefficient, α_c), and a classification of liquids based

 0021-9606/94/101(3)/2498/10/$6.00

on their α values was adopted;[21] namely, polar (associated) liquids with $(\alpha,\alpha_c)<1$ and nonpolar ones, with $(\alpha,\alpha_c)=1$. This classification led to various theoretical treatments[21] which attempted to explain values of $(\alpha,\alpha_c)<1$. Among these we mention the "entropy effects" and "orientation effects" theories where $(\alpha,\alpha_c)<1$ in polar liquids was attributed to restricted rotational freedom in the liquid in contrast to free rotation in the vapor, and the insufficient orientational relaxation of molecules approaching the phase boundary (from the bulk liquid phase or the vapor). However, a more recent critical examination of the experimental data and the above theories (as well as other), led Cammenga[21] to conclude, that $(\alpha,\alpha_c)=1$ for all pure liquids and "that the various theories predicting or explaining $(\alpha,\alpha_c)<1$ deserve only historical interest."

Applications of transition state theory (TST) to evaporation and condensation processes were reported to yield results in correspondence with experiments.[15,22–24] Under certain assumptions the TST expression obtained for the evaporation rate is[15]

$$G=\kappa\left(\frac{M}{2\pi RT}\right)^{1/2}\frac{RT}{N_A v_f e}\frac{Q_i^{\ddagger}}{Q_i}\,e^{-E^{\ddagger}/RT}, \tag{2}$$

where κ is the transmission coefficient, N_A is Avogadro's number, v_f is the free volume per molecule in the liquid, Q_i and $Q_i^{\ddagger}$ are the partition functions for internal degrees of freedom of a molecule in the liquid and activated complex, respectively, and $E^{\ddagger}$ is the activation energy for evaporation. In applying the above expression two assumptions were usually made: (i) $Q_i^{\ddagger}=Q_i$, implying that the internal molecular degrees of freedom are unaffected in going from the liquid phase to the transition state, and (ii) $E^{\ddagger}=E_v$, that is, identification of the activation energy for evaporation with the energy of evaporation (E_v). It has been pointed out[15] that the second (ii) assumption is incorrect and that E_v may be split into two terms, expressing the energy to bring a molecule from the interior of the liquid to the surface and the energy to remove it from the surface into the vapor phase. Only the later energy can be identified with the activation energy ($E^{\ddagger}$) for evaporation of a molecule from the surface. Aspects related to these two assumptions are investigated in our study.

To explore the energetics, structure, and dynamics of molecular mechanisms of evaporation processes of complex liquids we have used molecular dynamics simulations for two n-alkane liquids, n-C_6H_{14} (hexane) and n-$C_{16}H_{34}$ (hexadecane), thus allowing a detailed assessment of the chain-length dependence of the molecular mechanisms of evaporation processes.[25] Our results reveal that evaporation in these liquids occurs via a sequential segmental mechanism with the end segment of the molecule leaving the liquid surface first. Furthermore, our simulations show that for the short-chain alkane (n-C_6H_{14}) a certain fraction of the evaporating molecules leave the liquid surface in the form of dimers, with the majority leaving as monomers. We also find that for the shorter alkane (hexane) liquid about 10% of the collisions of vapor molecules with the liquid surface lead to backscattering into the vapor, while for hexadecane sticking of vapor molecules to the liquid surface is complete. In addition we find that molecular conformations are significantly changed upon evaporation. In particular, the *trans/gauche* ratio in hexadecane is decreased in going from the liquid to vapor phase, while the reverse is found for hexane.

Details of our MD simulations are given in Sec. II. In Sec. III, we describe and discuss the results of our simulations. Our findings are summarized in Sec. IV.

II. MOLECULAR DYNAMICS SIMULATIONS

In this study, we investigated n-C_6H_{14} and n-$C_{16}H_{34}$ films (thickness $d_{th}\sim 50$ and 45 Å, respectively) adsorbed on a crystalline substrate [modeling Au(001)] with the use of molecular dynamics simulations. The static crystalline substrate was set in the geometry of a (001) gold surface consisting of three layers, with the lattice parameter of gold (the dynamics of the gold surface appears to have no discernable effect on the properties of the liquid film). The areas of the calculational cells, which were periodically repeated in the $x-y$ directions parallel to the surface [with no periodicity applied along the film thickness direction (z)], were 3.745×10^3 Å^2 (i.e., a linear dimension of 61.2 Å). A reflecting wall was placed at $z=120$ Å above the solid surface to prevent molecules from escaping the system. The total number of molecules in the calculational cell were $N(C_6H_{14})=800$, and $N(C_{16}H_{34})=300$.

The alkane systems were described via intra- and intermolecular interactions developed previously,[3,5,25–27] including intersegment (CH_2 and CH_3 pseudoatoms) interactions, dihedral, and bond-bending potentials. The interactions between the pseudoatoms and the crystalline substrate were modeled via 6–12 Lennard-Jones potentials, with parameters ($\sigma=3.28$ Å and $\epsilon=0.429$ kcal/mol) determined by fitting to experimentally estimated adsorption energies.[5]

The equations of motion were integrated using Gear's fifth-order predictor–corrector algorithm[28] with a time step $\Delta t=1.5\times10^{-3}\ \tau$, where $\tau=1.93$ ps. The simulations were performed in the canonical ensemble, with the temperature controlled via infrequent scaling of particles' velocities.

In each simulation, we began with a careful preparation and a prolonged equilibration, which were described in detail elsewhere,[3,5] to generate an equilibrated liquid film at low temperature ($T=300$ K for n-C_6H_{14} and $T=350$ K for n-$C_{16}H_{34}$; the corresponding experimental boiling temperatures are $T_b=371$ and 560 K, respectively[29]). Subsequently, the systems were heated to the desired temperature via stochastic thermalization of the particles' velocities. The final temperatures were $T=334$ K (i.e., $0.9T_b$) and $T=554$ K (i.e., $0.99T_b$) for C_6H_{14} and $C_{16}H_{34}$, respectively. The preparation and equilibration lasted 2 ns. The heating process took another 470 ps, and the results reported here represented calculation for the last 300 ps. We note that our simulation times are very long by current MD standards for such complex systems.

III. RESULTS

In this section we present results of our simulations of adsorbed n-C_6H_{14} and n-$C_{16}H_{34}$ liquid films at 334 and 554 K, respectively. In the first part we discuss energetics, structural, and transport properties of the liquid–vapor interfaces

of the film. Results pertaining to the molecular mechanisms of evaporation and condensation processes are discussed in the second part of this section.

A. The liquid–vapor interface

Breaking the translational invariance of a liquid at interfaces (solid–liquid or liquid–vapor) modifies the density distribution and structure of the liquid in the vicinity of the interface. Such interfacial effects include oscillatory behavior of the liquid density[2] (so-called "liquid layering" or "liquid stratification," which is particularly pronounced at solid–liquid interfaces, although nonmonotonic density profiles have been reported also for liquid–vapor interfaces of liquid metals[30]) and interface induced orientational and conformational effects exhibited by molecular liquids (particularly, but not exclusively, complex liquids with a chain skeletal structure) at both solid–liquid (sl) and liquid–vapor (lv) interfaces.[3–6,10] In addition to these interfacial structural effects, transport properties of liquids are also modified near interfaces (e.g., the diffusion constant of hexadecane molecules in the solid–liquid interface is markedly smaller and that in the liquid–vapor interfacial region larger than that in the bulk[5]).

Segmental density profiles [$\rho(z)$] for n-hexane and n-hexadecane adsorbed films (at 334 and 554 K, respectively) plotted versus distance from the center of atoms in the first layer of the solid surface, are displayed in Figs. 1(a) and 2(a), respectively, and the scaled density profiles of the end (1 and 6 for C_6H_{14} and 1 and 16 for $C_{16}H_{34}$) and middle segments (3 and 4 for n-C_6H_{14} and 8 and 9 for n-$C_{16}H_{34}$) are shown in Fig. 3. In both cases the solid-to-liquid (sl) interface is characterized by a regularly spaced oscillatory profile of the film segmental density [see Figs. 1(a) and 2(a)], with the amplitude of the density oscillations decreasing away from the solid surface, and extending up to 18 Å into the film. (Curiously, the range of density oscillations in the adsorbed films is similar to the range of measured oscillatory forces between mica surfaces across hexadecane.[31]) The range of the density oscillations is similar to that found by us earlier for a lower temperature liquid n-hexadecane ($T=350$ K, see Ref. 5). Note that past the fourth oscillation, the density achieves a value similar to that of the corresponding bulk alkane liquid (e.g., for n-C_6H_{14} the calculated density in the middle region of the liquid film at 334 K is 0.62 g/cm^3 compared to an experimental value of 0.62±0.005 g/cm^3 for liquid hexane at 61 °C[29]). While the range and amplitude of the liquid density oscillations may depend somewhat on the nature of the liquid-to-solid interactions (bonding strength and other characteristics, such as angular dependent versus central force interaction, etc.) liquid layering at sl interfaces appears to be a general phenomenon characteristic of the nature of atomic and molecular packing of liquids near a solid boundary. We note, however, that surface roughness and/or complex molecular structures (such as branched molecules) may obliterate the sl density oscillations.[2]

From Fig. 3 we observe that various molecular segments occupy the lv interfacial region almost equally, with only a slight preference for end segments in the case of the n-hexadecane system to be found in the outermost region

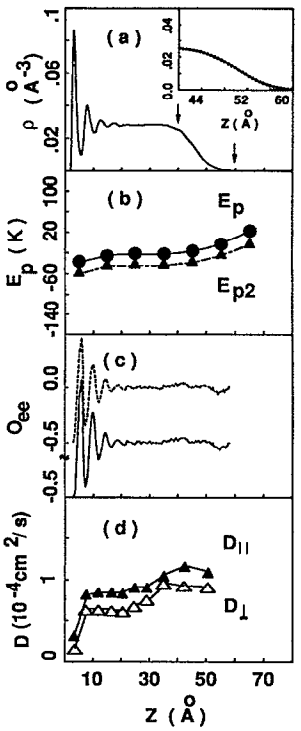

FIG. 1. Properties of a n-C_6H_{14} liquid film adsorbed on an Au(001) substrate, at 334 K. The segment density profile of the system plotted versus distance normal to the solid surface (z) is shown in (a), with the origin at the center of atoms in the top layer of the solid substrate. An error-function fit [see Eq. (3)] for the tail region (marked by arrows) is shown in the inset. (The fit parameters are $\rho_l=0.62$ g/cm^3, $\rho_v=0.003$ g/cm^3, $z_0=48.7$ Å, and $w_\rho=5.0$ Å; the width of the interface is given by $W=\sqrt{2}w_\rho$) Shown in (b) are segment potential energy profiles; total potential energy (E_p) and pairwise contributions (E_{p2}). Profiles of the molecular end-to-end vector order parameter, O_{ee} (solid line), as well as a modified, segmentally based, order parameter (Ref. 37), $O(z)$ (dashed line), is shown in (c), illustrating orientational preference of molecules in the solid-to-liquid interfacial region to lie parallel to the surface plane. Molecular diffusion constants in the direction parallel ($D_\parallel$) and perpendicular ($D_\perp$) to the surface plotted vs distance (z) are shown in (d).

(toward the vapor phase). A similar behavior was found in other simulations of the lv interfaces of alkanes, where a preferential occupation of the outermost region by end segments observed at low temperatures was greatly diminished upon heating.[14]

To determine the shape of the monotonically decreasing density profile at the liquid–vapor (lv) interface we use an error function fit to the lv tail region[5,33] of the data shown in Figs. 1(a) and 2(a),

$$\rho_s(z)=0.5(\rho_l+\rho_v)-0.5(\rho_l-\rho_v)\times\mathrm{erf}[(z-z_0)/(2w_\rho^2)^{1/2}]. \quad (3)$$

From the fits, shown as insets to Figs. 1(a) and 2(a), we determine that the interface width parameter w_ρ (the interface width is given by $W=\sqrt{2}w_\rho$) for the hexadecane film at 554 K is $w_\rho=5.15$ Å (compared to $w_\rho=2.95$ Å determined at 350 K;[5] a similar trend of increasing lv interface width of n-alkanes with temperature was observed recently using x-ray reflectivity measurements[34]), and that for the hexane film $w_\rho=5.0$ Å at 334 K.

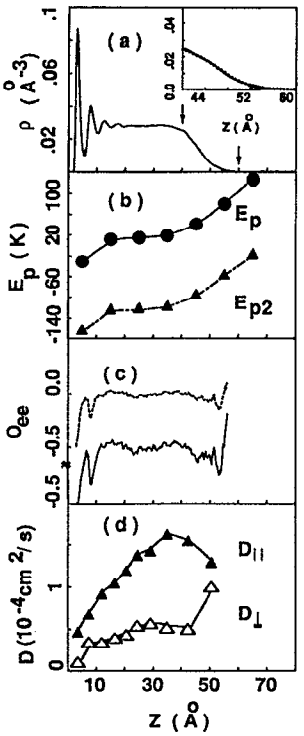

FIG. 2. Same as Fig. 1, for a n-$C_{16}H_{34}$ liquid film adsorbed on an Au(001) surface at 554 K. The error-function fit parameters [see Eq. (3)] used in the inset to (a) were $\rho_l=0.67$ g/cm^3, $\rho_v=0.004$ g/cm^3, $z_0=44.2$ Å, and $w_\rho=5.15$ Å. The large anisotropy between $D_{||}$ and $D_\perp$ in the middle region of the film (panel d) is due to the finite thickness of the film, and the sharp increase of $D_\perp$ in the lv interfacial region may be attributed to molecules attempting to evaporate from the liquid.

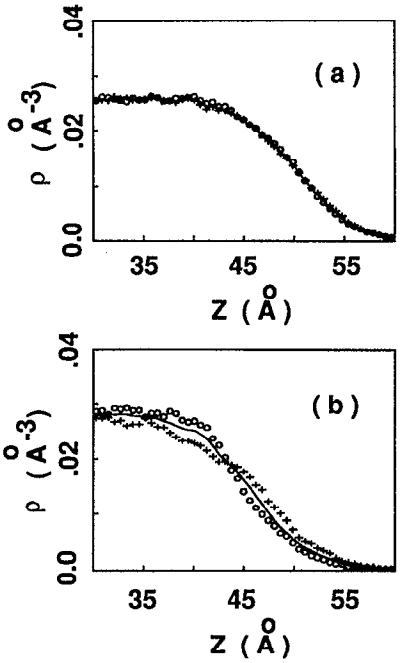

FIG. 3. Scaled density profiles of the end segments (+), middle segments (○), and total hydrocarbon (—) of (a) hexane at $T=334$ K and (b) hexadecane at $T=554$ K. Shown here are the density profiles near the liquid–vapor interface region of the films.

The liquid-to-vapor interface of the films appears "rough" on the molecular scale. The equilibrium average segmental distributions of the z-height fluctuations for the films can be fitted well by Gaussians $(w\sqrt{2\pi})^{-1}\exp[-(z-z_0)^2/2w^2]$ with $w\simeq4.95$ and 5.11 Å for n-C_6H_{14} and $C_{16}H_{34}$, respectively. It is interesting to note that the joint observation of a Gaussian height distribution and an error-function density profile of the lv interface may imply a short correlation length at the surface region of the molecular liquid film.[33] In this context we remark that the shape of the lv interfacial density tail of long-chain molecules (polymers) is predicted to obey a $z^{-\mu}$ law with $\mu=4/3$ on the basis of a self-similarity argument,[35] or $\mu=2$.[36] The question at what size a crossover to the long-chain regime occurs remains open.

The energetics of the adsorbed films are shown in Figs. 1(b) and 2(b) where the total potential energies, E_p (including dihedral, bond-bending, and pairwise intramolecular and intermolecular interactions, as well as the pairwise contribution due to interaction with the crystalline substrate), as well as the sum of only the pairwise interactions (E_{p2}), are plotted versus the center of mass distances of the molecules from the solid surface. These results demonstrate the effect of the attractive interaction with the substrate, as well as the increase in potential energy in the liquid–vapor transition region, and ultimately in the vapor.

We denote by $\Delta_s^{lv}=(E_p^v-E_{p,l}^s)/n$ the per-segment (where n is the number of segments in C_nH_{2n+2}) difference between the average per-molecule potential energies in the vapor (E_p^v) and at the surface of the liquid ($E_{p,l}^s$), and by $\Delta_s^l=(E_{p,l}^s-E_{p,l})/n$ the per-segment difference between the average per-molecule potential energies at the surface of the liquid and in the bulk (middle) region of the liquid film ($E_{p,l}$). With these definitions $\Delta^{lv}=(E_p^v-E_{p,l})/n=\Delta_s^{lv}+\Delta_s^l$ is the per-segment difference between the average potential energies in the vapor and bulk liquid. From Table I we observe that the increases in potential energy upon evaporation are of similar magnitudes for the two liquids. Furthermore the increase in potential energy between the bulk liquid and the surface (Δ_s^l) is a significant fraction of Δ^{lv}, correlating with the arguments used in modern applications[15] of TST to evaporation processes (see Sec. I). Additionally, we find that

TABLE I. Potential energies (in degrees Kelvin, K) for the liquid n-C_6H_{14} and n-$C_{16}H_{34}$ at 334 and 554 K, respectively. $E_{p,l}$, $E_{p,l}^s$, and E_p^v are the per-molecule potential energies at the middle of the liquid film, at the liquid–vapor interfacial region, and in the vapor, respectively. The energy differences per segment (i.e., differences of potential energies divided by $n=6$ for hexane and $n=16$ for hexadecane) are defined as: $\Delta_s^{lv}=(E_p^v-E_{p,l}^s)/n$, $\Delta_s^l=(E_{p,l}^s-E_{p,l})/n$ and $\Delta^{lv}=(E_p^v-E_{p,l})/n$.

	C_6H_{14}	$C_{16}H_{34}$
$E_{p,l}$ (K)	−1858	313
$E_{p,l}^s$ (K)	−698	3089
E_p^v (K)	1267	9404
Δ_s^{lv} (K)	328	395
Δ_s^l (K)	193	174
Δ^{lv} (K)	511	569

TABLE II. Results for n-C_6H_{14} at $T=334$ K for density ρ, gyration radii ($R^2_{g,xy}$ parallel to the solid surface, $R^2_{g,z}$ the component normal to the surface, and $R^2_g=R^2_{g,xy}+R^2_{g,z}$), end-to-end length ($R^2_{ee,xy}$ parallel to the surface, $R^2_{ee,z}$ normal to the surface, and $R^2_{ee}=R^2_{ee,xy}+R^2_{ee,z}$), percent trans and gauch configurations, and the orientational order parameter O_{ee}. The results are given for various regions of the adsorbed liquid film; the solid-to-liquid interface (sl), the middle region of the film (middle), the liquid-to-vapor interface (lv), and in the vapor.

	sl	Middle	lv	Vapor
ρ (g/cm^3)	1.79	0.62	0.30	0.0028
$R^2_{g,xy}$ (Å^2)	4.23	2.74	2.73	2.54
$R^2_{g,z}$ (Å^2)	0.20	1.40	1.40	1.36
R^2_g (Å^2)	4.43	4.14	4.13	3.90
$R^2_{ee,xy}$ (Å^2)	33.57	20.71	20.65	17.77
$R^2_{ee,z}$ (Å^2)	0.35	10.60	10.53	10.52
R^2_{ee} (Å^2)	33.92	31.31	31.18	28.19
Trans (%)	70.80	71.77	70.70	82.85
Gauch(+) (%)	15.30	14.42	14.80	10.0
Gauch(−) (%)	13.90	13.81	14.50	7.15
O_{ee}	−0.48	0.0	0.0	

the surface tension for the n-$C_{16}H_{34}$ liquid film at 554 K is $\sigma\simeq 14$ dyn/cm, compared to $\simeq 22$ dyn/cm determined previously[5] at 350 K (in close agreement with an experimental value[32] at 80 °C of 22.58±0.1 dyn/cm); for the n-C_6H_8 liquid film we determine $\sigma=9.0$ dyn/cm at 334 K and $\sigma=16.7$ dyn/cm at 300 K, compared to experimentally determined values of 14.1±0.1 dyn/cm and 17.7±0.1 dyn/cm, respectively.[32]

Large molecular structural effects occur at the solid-to-liquid interface[5] [these effects are particularly pronounced for the longer-chain alkane (n-$C_{16}H_{34}$)]. As seen from Tables II and III and Figs. 1(c) and 2(c) the molecules at the sl interface are oriented preferentially with their axis parallel to the surface [see the order parameter $O_{ee}(z)=1/2\langle(3\cos^2\theta-1)\rangle$, where $\cos(\theta)=\mathbf{R}_{ee}(z)\cdot\hat{z}/|\mathbf{R}_{ee}(z)|$ and $\mathbf{R}_{ee}(z)$ is the end-to-end vector for a molecule whose center of mass is located in a narrow interval δz about z,[37] in Tables II and III and Figs. 1(c) and 2(c)], and the components of their radii of gyration and end-to-end distance vector parallel to the surface ($R_{g,xy}$ and $R_{ee,xy}$) are significantly larger than those in the direction normal to the surface. The total gyration radii and end-to-end distances for molecules at the sl interfacial region are larger than those in the bulk of the film, indicating that the adsorbed molecules at this region

TABLE III. Results for n-$C_{16}H_{34}$ at $T=554$ K (see caption to Table II).

	sl	Middle	lv	Vapor
ρ (g/cm^3)	2.05	0.67	0.29	0.0042
$R^2_{g,xy}$ (Å^2)	25.52	14.26	15.24	12.95
$R^2_{g,z}$ (Å^2)	0.15	7.01	5.91	7.67
R^2_g (Å^2)	25.67	21.27	21.15	10.62
$R^2_{ee,xy}$ (Å^2)	237.87	117.94	128.28	96.0
$R^2_{ee,z}$ (Å^2)	0.56	58.46	44.90	67.79
R^2_{ee} (Å^2)	283.43	176.40	173.18	163.79
Trans (%)	65.60	65.49	67.0	32.82
Gauch(+) (%)	16.09	17.35	16.63	31.40
Gauch(−) (%)	18.31	17.16	16.37	35.78
O_{ee}	−0.50	0.0	0.0	

are more extended (stretched). In this context we note that at the lv interface only mild orientational anisotropy is observed[14] at these high temperatures [more noticeable for the longer alkane, see Fig. 2(c)].

Effects of the interfaces on conformational properties of the alkane liquids are summarized in Tables II and III. We note first that for both hot alkane liquids the distributions of *trans* (t) and *gauche* (g_+ and g_-) dihedral configurations are nearly the same throughout the liquid; i.e., at both the middle of the liquid film as well as the interfacial regions $(t,g_+,g_-)=(72,14,14)$ for n-C_6H_{14}, and $(t,g_+g_-)=(66,17,17)$ for n-$C_{16}H_{34}$. This should be contrasted with our earlier findings for n-$C_{16}H_{34}$ at 350 K, where the percent *trans* configurations in the first adsorbed liquid layer was markedly higher (79,11,10) than in the bulk and lv tail (66,17,17). On the other hand, n-$C_{16}H_{34}$ molecules in the vapor phase possess an almost uniform distribution (33,31,36), characterized by a large decrease in the percent *trans* and corresponding increase in *gauche* configurations compared to that in the liquid. The reverse trend is found for n-C_6H_{14} where the percent trans configuration of vapor molecules is increased (83,10,7) compared to the liquid phase.[38]

The molecular structural modifications occurring upon evaporation are also reflected in the molecular radii of gyration (R_g) and end-to-end intramolecular distances (R_{ee}). From Tables II and III we find that the ratio between the radii of gyration of vapor and liquid molecules of n-$C_{16}H_{34}$ is $R_{g,v}/R_{g,l}\simeq 0.94$, and $R_{ee,v}/R_{ee,l}=0.96$, with very similar results for n-C_6H_{14}. These results indicate that gas-phase alkane molecules assume somewhat more compact molecular configurations in order to increase intramolecular intersegment attraction.

The variations in intramolecular structure between vapor and liquid molecules, together with expected variations in vibrational and rotational properties in the two phases, indicate that accurate determination of equilibrium evaporation (and condensation) constants, would require incorporation of these effects in the corresponding partition functions which enter the TST equation [see Eq. (2)].

Finally, we note that the molecules in the films exhibit liquid like, markedly inhomogeneous diffusion constant profiles [see Figs. 1(d) and 2(d)], with both the diffusion constants in the directions parallel ($D_\parallel$) and normal ($D_\perp$) to the solid surface markedly diminished in the sl interfacial region (note that for both systems $D_\parallel > D_\perp$). We also remark that the diffusion constants for n-$C_{16}H_{34}$ calculated from our present high-temperature ($T=554$ K) simulations are significantly larger than those obtained from simulations at a lower temperature[5] ($T=350$ K).

B. Evaporation mechanisms

During our prolonged simulations of the hot alkane films a number of molecular evaporation events occurred (48 for n-C_6H_8 and 10 for n-$C_{16}H_{34}$). As mentioned in Sec. II a reflective boundary was placed at $z=120$ Å above the solid surface, which merely reverses the sign of the normal (z) component of a vapor molecule upon its collision with the boundary (specular scattering). As a result of such reflections, as well as intermolecular collisions in the vapor, most

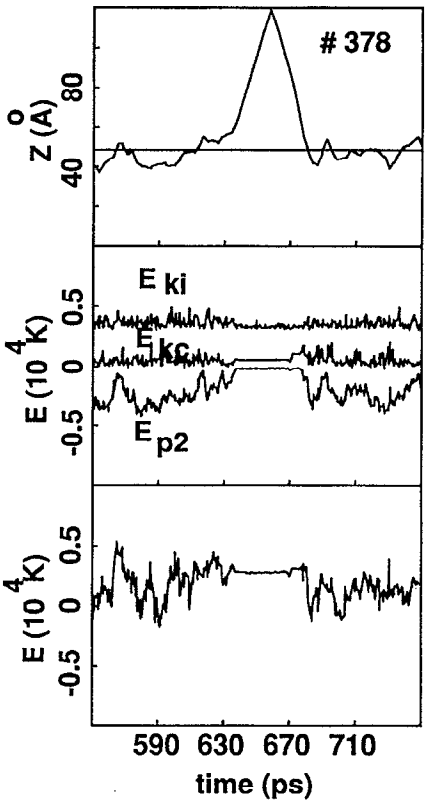

FIG. 4. Top: trajectory of the z position (normal to the surface) of the center of mass of an evaporating n-C_6H_{14} molecule (No. 378), plotted versus time, illustrating evaporation, reflection from the boundary of the system and readsorption into the liquid surface. The location of the Gibbs dividing surface is denoted by a horizontal line. Middle: internal vibrational (E_{ki}) and center-of-mass (E_{kc}) kinetic energies, and the pairwise contribution to the potential energy (E_{p2}) of the molecule, plotted versus time. Bottom: the total energy of the molecule vs time.

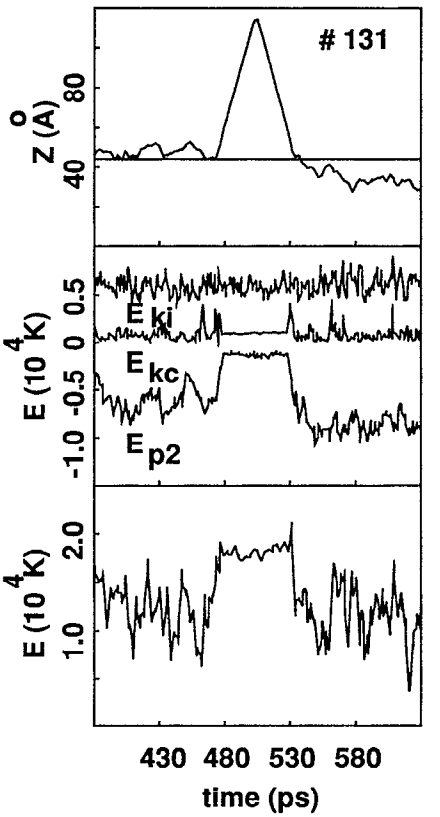

FIG. 5. Same as Fig. 4, for an evaporating n-$C_{16}H_{34}$ molecule (No. 131).

of the vapor molecules have collided back with the liquid surface leading to condensation or reflection back to the vapor (the condensation coefficients were determined to be close to unity for both systems; $\alpha_c \approx 1$ for n-$C_{16}H_{34}$ and $\alpha_c \approx 0.9$ for n-C_6H_{14}).

Inspection of the trajectories of evaporating molecules reveals various events, including evaporation of monomers, dimers, dissociation of gas-phase dimers by collision with vapor molecules, and condensation or backscattering from the liquid surface. In the following we illustrate these processes using selected representative trajectories.

In the case of the shorter alkane (n-C_6H_{14}) out of 48 molecular evaporation events, 38 consisted of monomer evaporations, and in 5 cases dimers were evaporated. For n-$C_{16}H_{34}$ all the evaporating molecules left the liquid surface as monomers. Representative trajectories (molecular center of mass versus time) corresponding to monomer evaporation and subsequent condensation are shown in Figs. 4(a) and 5(a) for n-C_6H_{14} and n-$C_{16}H_{34}$, respectively, along with the internal vibrational (E_{ki}) and center of mass (E_{kc}) kinetic energies of the molecule, the pairwise contribution to the molecule's potential energy (E_{p2}), and the total energy (E) of the molecule [Figs. 4(b), 4(c) and 5(b), 5(c)]. The main trends which we observe in the energetics of the molecules are rather fast increase in the potential energy of the molecule during evaporation and a decrease upon condensation. During the "free flight" period fluctuations in the total energy of the molecule are due to interactions with other vapor molecules.

To explore details of the monomer evaporation mechanism we show in Figs. 6 and 7 (for n-C_6H_{14} and n-$C_{16}H_{34}$, respectively), the number of free segments (n_{seg}) of the molecules versus time, recorded during the evaporation (a) and condensation processes (b). These plots were obtained by recording for a given molecule the number of segments, ver-

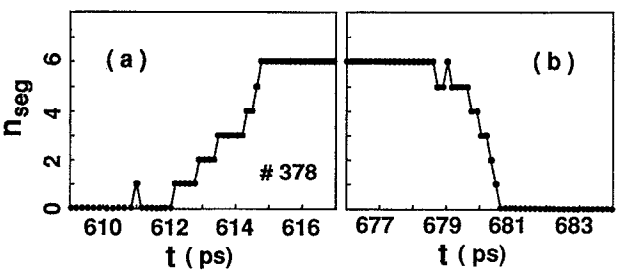

FIG. 6. Number of free segments (i.e., segments of the evaporating molecule found above a plane located at $z_0 + w_\rho$, where z_0 is the position of the Gibbs dividing surface and w_ρ the halfwidth of the liquid-to-vapor interface) for a n-C_6H_{14} molecule (No. 378, see Fig. 4), plotted vs time. Sequential segmental evaporation of the molecule is illustrated in (a) and condensation back into the liquid film in (b).

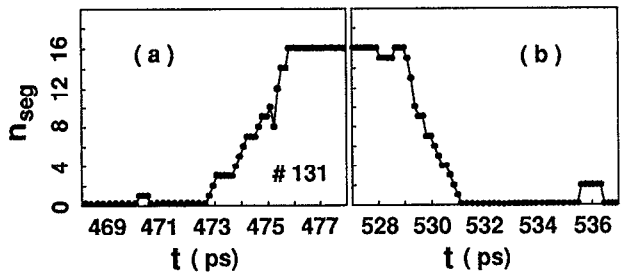

FIG. 7. Same as Fig. 6, for an evaporating n-$C_{16}H_{34}$ molecule (No. 131, see Fig. 5).

sus time, which are found above a plane located at $z_0+\sqrt{2}W/2$, where z_0 is the position of the Gibbs dividing surface and W is the lv interface width [see Figs. 1(a) and 2(a), and Eq. (3)]. In all cases evaporation was observed to occur starting with an end segment of the molecule leaving the liquid surface. Subsequently, the other segments are sequently "dragged" out of the liquid. As seen from Figs. 6 and 7 the sequential segmental evaporation processes occur over ~3 ps for both liquids. Condensation of the molecules is somewhat faster and less segmental in nature. Atomic configurations illustrating the dynamics of an evaporation process of a hexadecane molecule are shown in Fig. 8.

A trajectory of an n-C_6H_{14} molecule illustrating evaporation, backscattering from the liquid surface and eventual condensation is shown in Fig. 9(a) and the corresponding energetics in Figs. 9(b) and 9(c). This molecule started deeper in the liquid, and its approach and traversal of the lv interface is accompanied by increase in its total energy leading to evaporation. As seen the backscattering from the liq-

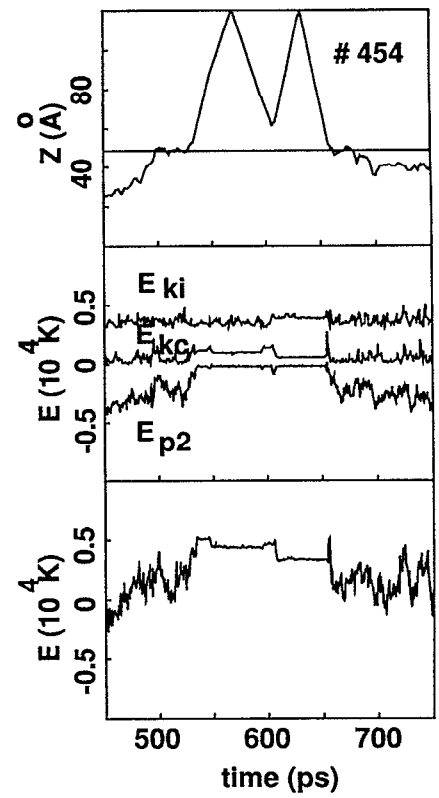

FIG. 9. Same as Fig. 4 for an C_6H_{14} molecule (No. 454) illustrating evaporation, backscattering from the liquid and eventual condensation into the liquid.

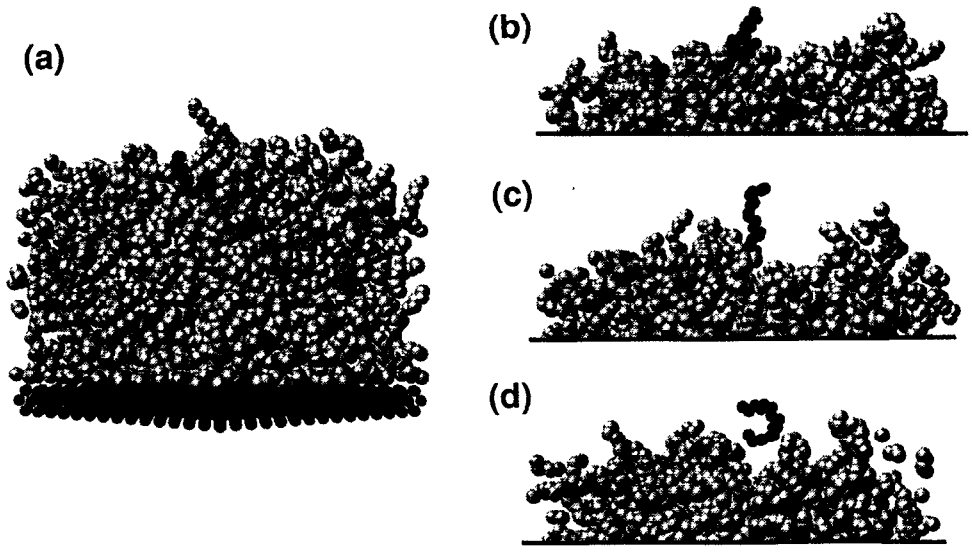

FIG. 8. Atomic configurations at selected times during the evaporation process of an n-$C_{16}H_{34}$ molecule (No. 131), illustrating the sequential segmental evaporation mechanism. Note the change in the molecular configuration upon evaporation (d). The configurations shown were recorded 2.9 ps apart. In (a) a side view of the whole system is shown with the solid substrate at the bottom. In (b)–(d) only the pertinent top part of the liquid film is shown. The evaporating molecule is depicted darker than the other molecules in the film.

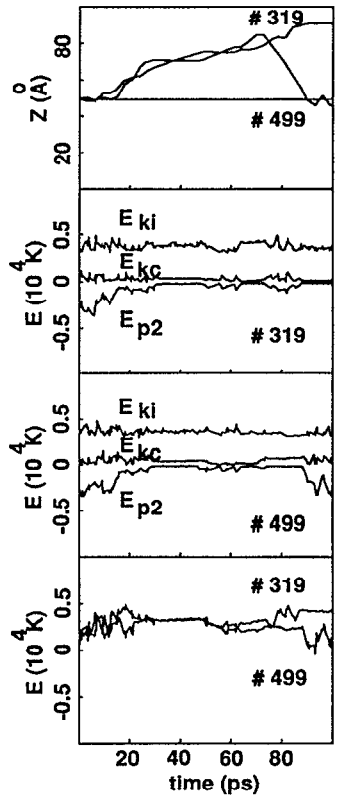

FIG. 10. Evaporation of an n-C_6H_{14} dimer (molecules No. 319 and No. 499). Trajectories of the z position (normal to the surface) of the centers of mass of the two molecules, plotted vs time, are shown at the top, illustrating dimer evaporation, spontaneous dissociation of the dimer, and condensation into the liquid of molecule No. 499. The bottom panels show the time development of the internal (E_{ki}) and center-of-mass (E_{kc}) kinetic energies, the pairwise contributions to the potential energy (E_{p2}), and the total energies, of the two molecules.

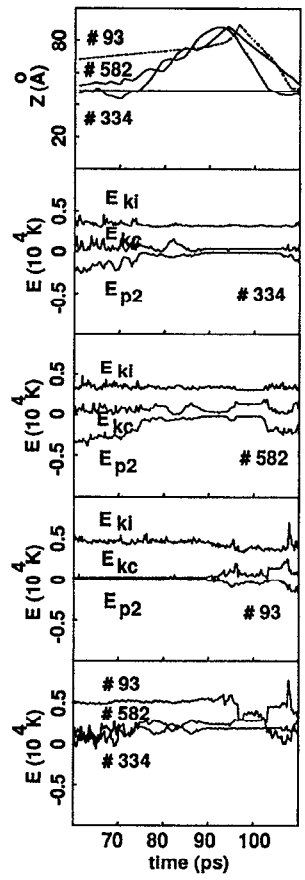

FIG. 11. Same as Fig. 10, illustrating formation of an n-C_6H_{14} dimer (molecules No. 334 and No. 482) via dragging of one of the molecules (No. 334) by a quasifree one (No. 582). Also shown is the trajectory and energies of an n-C_6H_{14} molecule (No. 93) which collides with the dimer, and causes dissociation and eventual condensation.

uid surface (at ~600 ps) is inelastic, resulting in a somewhat reduced center-of-mass velocity of the scattered vapor molecule.

Evaporation of dimer molecules has been recently observed in molecular beam experiments on carboxylic acid,[39] and in MD simulations of methanol.[25] In both bases stabilization of dimers by hydrogen bonding may be invoked to rationalize such dimer evaporation processes. Surprisingly we have also observed dimer evaporation processes in our simulations of alkane liquids where no hydrogen bonding occurs. Examples of such events are shown for n-C_6H_{14} in Figs. 10 and 11, while dimer formation in the vapor phase is illustrated for n-$C_{16}H_{34}$ in Fig. 12.

In the dimer evaporation event illustrated in Fig. 10 the hexane dimer was "preformed" at the lv interface prior to evaporation, with the two molecules leaving the surface simultaneously. About 70 ps later the dimer spontaneously dissociated leading to collision and condensation at the liquid surface of one of the molecules (No. 499), while the other remains in the gas phase.

A more complex sequence of events is shown in Fig. 11. In this case dimer evaporation occurs via a mechanism where at the beginning of the process one of the hexane molecules (No. 582) is in a "quasifree" state translating parallel to the liquid surface. During its motion it interacts with molecules of the liquid surface, leading to dragging of one of them (No. 334) and resulting in formation of a bound vapor dimer molecule. The free flight of the dimer was interrupted later by a collision with a vapor phase monomer (No. 93) which led to dissociation of the dimer and eventual condensation of all three molecules.

Finally, in the context of dimer formation, we show in Fig. 12 trajectories and energetics for n-$C_{16}H_{34}$, illustrating monomer evaporation (No. 40) followed by collision in the vapor with another vapor molecule (No. 106), leading to the formation of a gas-phase dimer which remains bound for about 20 ps and then dissociates, resulting in condensation of one of the molecules (No. 106).

IV. SUMMARY

In this study we have investigated energetic, structural and dynamic properties of adsorbed liquid alkane films (n-C_6H_{14} and n-$C_{16}H_{34}$) at high temperatures, focusing on the dynamics and molecular mechanisms of evaporation. Our molecular dynamics simulations show that characteristics of the solid-to-liquid (sl) interfaces of these liquids, studied previously for low-temperature liquid hexadecane films,[5]

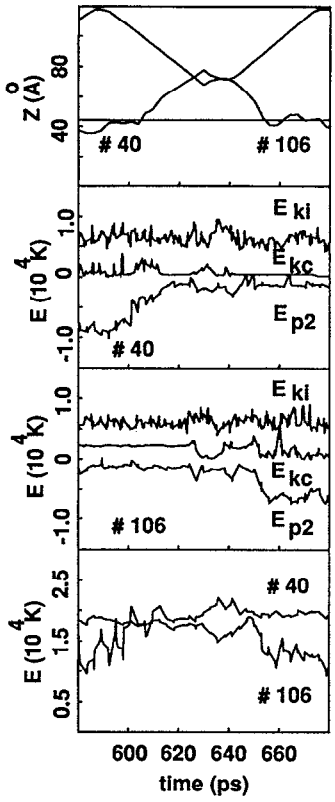

FIG. 12. Trajectories and energies (see Fig. 4) for two n-$C_{16}H_{34}$ molecules, illustrating evaporation of one of the molecules (No. 40), its subsequent collision with a vapor hexadecane molecule (No. 106) leading to formation of a vapor-phase dimer which is bound for ~20 ps. Eventually the dimer dissociates and one of the molecules (No. 106) condensates into the liquid.

[such as oscillations of the liquid density in the direction normal to the solid surface (layering), preferential orientation of molecules in the vicinity of the solid surface, with the molecular axis parallel to the surface plane, and markedly reduced diffusion of molecules in that region] persist at high temperatures. We have also found that properties of the high-temperature liquid-to-vapor (lv) interfaces of these liquids are similar in nature to those observed at lower temperatures,[5] exhibiting an increase of the width of the lv interfacial region.

Our main results pertaining to molecular evaporation processes may be summarized as follows:

(i) The molecular evaporation mechanism is cooperative and sequential in nature, starting with an end segment of a molecule and proceeding via sequential segment-by-segment evaporation of the molecule (see Figs. 6–8).

(ii) Evaporation is accompanied by marked molecular conformational changes. For n-$C_{16}H_{34}$ molecules in the vapor the trans and gauch conformations are distributed almost equally [i.e., $(t,g_+,g_-)=(33,31,36)$] while in the hot liquid the fraction of trans conformations is much larger [i.e., $(t,g_+,g_-)=(66,17,17)$]. For n-C_6H_{14} a reverse trend was found with the fraction of *trans* conformations larger in the vapor [i.e., $(t,g_+,g_-)=(83,10,7)$] than in the hot liquid [i.e., $(t,g_+,g_-)=(72,14,14)$]. These conformational changes are also reflected in variations occurring upon evaporation in the molecular radius of gyration and end-to-end distances (see Tables II and III).

(iii) In the case of the shorter alkane (hexane) a certain fraction of the evaporation events occurred via dimers. Transient dimerization in the vapor phase was also observed.

(iv) The condensation coefficients of vapor molecules into the liquid were found to be close to unity for both alkane liquids.

(v) The energy required to transfer a molecule from inside the liquid to the interfacial liquid-to-vapor region is a significant fraction of the total energy required to transfer a molecule from inside the liquid to the vapor (see Table I).

These results have certain implications for theoretical treatments of equilibrium evaporation rate constants (e.g., considerations pertaining to the nature of the transition state, the energetics of the process, and the conformational changes between liquid and vapor molecules in applications of transition state theory to evaporation processes of complex liquids[21]), and provide the impetus for further theoretical and experimental investigations of the molecular mechanisms of evaporation of complex liquid systems.

ACKNOWLEDGMENTS

Work supported by the National Science Foundation, the Air Force Office for Scientific Research, and the U.S. Department of Energy. Simulations performed at the Pittsburgh Supercomputer Center.

[1] A. W. Adamson, *Physical Chemistry of Surfaces* (Wiley, New York, 1982).
[2] J. N. Israelachvili, *Intermolecular and Surface Forces* (Academic, London, 1985), p. 158.
[3] M. W. Ribarsky and U. Landman, J. Chem. Phys. **97**, 1937 (1992), and references to earlier work therein.
[4] U. Landman, W. D. Luedtke, J. Ouyang, and T. K. Xia, Jpn. J. Appl. Phys. **32**, 1444 (1993).
[5] T. K. Xia, J. Ouyang, M. W. Ribarsky, and U. Landman, Phys. Rev. Lett. **69**, 1967 (1992).
[6] W. D. Luedtke and U. Landman, Comput. Mater. Sci. **1**, 1 (1992).
[7] (a) S. Granick, Science **253**, 1374 (1991); (b) S. Granick, in *Physics of Polymer Surfaces and Interfaces*, edited by I. C. Sanchez (Butterworth-Heinemann, Boston, 1992), p. 227, and references therein.
[8] T. K. Xia and U. Landman, Science **261**, 1310 (1993), and references therein.
[9] X. Z. Wu, E. B. Sirota, S. K. Sinha, B. M. Ocko, and M. Deutsch, Phys. Rev. Lett. **70**, 958 (1993).
[10] T. K. Xia and U. Landman, Phys. Rev. B **48**, 11 313 (1993).
[11] P. A. Thompson and M. O. Robbins, Science **250**, 792 (1990).
[12] See articles in *Fundamentals of Friction: Macroscopic and Microscopic Processes*, edited by I. L. Singer and H. M. Pollock (Kluwer, Dordrecht, 1992).
[13] R. J. Hunter, *Foundations of Colloid Science* (Oxford University, Oxford, 1987 and 1989), Vols. 1 and 2.
[14] J. G. Harris, J. Phys. Chem. **96**, 5077 (1992).
[15] H. K. Cammenga, in *Current Topics in Materials Science*, edited by E. Kaldis (North-Holland, Amsterdam, 1980), Vol. 5, p. 335, and references therein.
[16] J. Dalton, Gilberts Ann. Phys. **15**, 121 (1803).
[17] J. Stefan, Wiener Akad. Ber. **68**, 383 (1873).
[18] H. Hertz, Ann. Phys. **17**, 177 (1882).
[19] I. Langmuir, Phys. Rev. **2**, 329 (1913); **8**, 149 (1916); Phys. Z. **14**, 1273 (1913); J. Am. Chem. Soc. **38**, 2221 (1916).
[20] R. W. Schrage, *A Theoretical Study of Interphase Mass Transfer* (Columbia University, New York, 1953); see other references in Ref. 15.
[21] See critical discussion in Ref. 15.
[22] J. F. Kincaid and H. Eyring, J. Chem. Phys. **6**, 620 (1938).

[23] E. M. Mortensen and H. Eyring, J. Phys. Chem. **64**, 846 (1960).
[24] H. Eyring and E. M. Eyring, *Modern Chemical Kinetics*, 2nd ed. (Reinhold, New York, 1967).
[25] M. Matsumoto and Y. Kataoka, Phys. Rev. Lett. **69**, 3782 (1992).
[26] J. P. Ryckaert and A. Bellmans, Discuss. Faraday Soc. **66**, 95 (1978).
[27] S. Leggeter and D. J. Tildesley, Mol. Phys. **68**, 519 (1989).
[28] M. P. Allen and D. J. Tildesley, *Computer Simulations of Liquids* (Clarendon, Oxford, 1987).
[29] N. L. Allinger, M. P. Cava, D. C. De Jongh, C. R. Johnson, N. A. Lebel, and C. L. Stevens, *Organic Chemistry* (Worth, New York, 1971), p. 25; R. W. Gallant, *Physical Properties of Hydrocarbons* (Gulf, Houston, 1968), Vol. 1, Chap. 15; N. B. Vargraftik, *Tables of the Thermophysical Properties of Liquids and Gases*, 2nd ed. (Halsted, New York, 1975).
[30] E. T. Chen, R. N. Barnett, and U. Landman, Phys. Rev. B **41**, 439 (1990).
[31] See H. K. Chistenson, D. W. R. Gruen, R. G. Horn, and J. N. Israelachvili, J. Chem. Phys. **87**, 1834 (1987), in the context of surface force measurements of confined liquid *n*-hexadecane.
[32] J. J. Jasper, J. Phys. Chem. Ref. Data **1**, 841 (1972), see Table 51.2.
[33] J. D. Weeks, J. Chem. Phys. **67**, 3106 (1977).
[34] B. M. Ocko, X. Z. Wu, E. B. Sirota, S. K. Sinha, and M. Deutch, Phys. Rev. Lett. **72**, 242 (1994).
[35] P. G. de Gennes, *Scaling Concepts in Polymer Physics* (Cornell University, Ithaca, 1979); P. G. de Gennes and P. J. Pincus, J. Phys. (Paris), Lett. **44**, L241 (1983).
[36] E. Eisenreigler, K. Kremer, and K. Binder, J. Chem. Phys. **77**, 6296 (1982).
[37] Similar results [shown as dashed lines in Figs. 1(c) and 2(c)] were obtained using a modified definition of the orientational order parameter (Ref. 14), where $O(z)=1/2\langle 3\cos^2\psi-1\rangle$ and ψ is the angle between the unit vector $\hat{z}$ and a vector connecting a pair of carbon atoms that are two units apart in a molecule (e.g., atoms n and $n+2$). The value of the order parameter is calculated for each molecule in the film and is plotted vs the location of the center of mass of the molecule.
[38] A similar tendency for slight shift toward the gauche state in going from the ideal gas to a dense fluid of butane was observed in R. Edberg, D. J. Evans, and G. P. Morriss, J. Chem. Phys. **84**, 6933 (1986).
[39] M. Faubel and Th. Kisters, Nature (London) **339**, 527 (1989).